UV-curable inorganic precursors enable direct 3D printing of SiOC ceramics

Hippolyte Dory, Philippe Miele, Chrystelle Salameh

Received: 30 April 2022 | Revised: 11 July 2022 | Accepted: 31 July 2022

DOI: 10.1111/ijac.14173

International Journal of Applied Ceramic Technology

SPECIAL ISSUE ARTICLE

UV-curable inorganic precursors enable direct 3D printing of SiOC ceramics

Hippolyte Dory[1] | **Philippe Miele**[1,2] | **Chrystelle Salameh**[1]

[1]Institut Européen des Membranes, IEM, UMR 5635, Univ Montpellier, ENSCM, CNRS, Montpellier, France

[2]Institut Universitaire de France (IUF), Paris Cedex 05, France

Correspondence
Chrystelle Salameh, Institut Européen des Membranes, IEM, UMR 5635, Univ Montpellier, ENSCM, CNRS, Montpellier, France.
Email: chrystelle.salameh@enscm.fr

Abstract

3D ceramic parts are of great interest for various applications including aerospace, defense, electronics, photonics, and biomedical. Yet, additive manufacturing of ceramics is challenging due to their poor machinability. Herein, two approaches based on the chemical modification of silicon resins to obtain UV-curable preceramic precursors of SiOC are described. The dual functionality of the synthesized resins acting both as preceramic precursor and as photopolymerizable entity under UV light is exploited. A set of characterization techniques has allowed the investigation of the mechanisms involved in the synthesis of the inorganic SiOC precursors according to the following approaches: (1) blend of the silicon resin with photoactive monomers and (2) synthesis of a single source UV-curable preceramic silicon resin. A correlation between the nature of the precursor and the properties of the derived SiOC is analyzed. From a technological point of view, the materials can be fabricated as dense or crack-free porous customized objects with low mass loss and optimal surface quality.

KEYWORDS
additive manufacturing, photopolymerization, polymer precursor, silicon oxycarbide

1 | INTRODUCTION

Ceramics have gained a lot of interest in the last two decades owing to their various properties such as good thermal and chemical stability, high mechanical strength, and oxidation resistance.[1] The most commonly used ceramics for technological, medical or environmental applications are metal oxides such as alumina, silica, yttria, or zirconia.[2,3] However, those ceramics are sensitive to harsh chemical environments, the use of silicon and carbon-based ceramics is rather preferable. In particular, silicon oxycarbide (SiOC), with improved chemical stability and mechanical properties when compared to silica, is becoming an increasingly attractive ceramic. SiOC presents luminescence properties,[4–6] high temperature viscoelasticity,[7] and crystallization resistance.[8] It can be produced from thermal conversion of silicon-based polymer precursors through the polymer-derived ceramics (PDC) route. Depending on the stoichiometry of SiOC, carbon content, pyrolysis atmosphere and temperature, physical properties can be tuned. SiOC ceramics have generally high density, hardness, and temperature resistance. They consist in two major phases where Si-C/Si-O bonds coexist together with an amorphous carbon phase.[9] The

presence of an excess of free carbon will inhibit the formation of crystalline SiC until 1500°C, stabilizing thus the amorphous structure of SiOC. At low free carbon content, the structure of SiOC glass is closer to silica, and the chemical durability decreases when exposed to alkaline and hydrofluoric media.[10,11]

Most of the preceramic precursors consist of silicon-based inorganic/organometallic molecules. A wide range of PDCs can be produced ranging from binary (SiC, Si_3N_4, BN, AlN[12,13]) to ternary (BCN, SiOC, SiCN[14]) and quaternary (SiAlON, SiAlCN,[15] SiBCN[16]) systems. They can be synthesized at relatively low temperatures (1000–1300°C) compared to classical powder technology (above 1700°C) with a lower energy consumption. Moreover, the use of polymer/molecular precursors allows an easy tailoring of the chemical composition and a controlled nanostructure during polymerization and thermal treatment.[17]

The greatest advantage of this class of materials is their easy shaping and processing using conventional polymer-forming technologies such as coating, spinning, infiltration, extrusion, or injection molding. However, more complex ceramic architectures are provided by additive manufacturing (AM) technologies enabling the design of intricate geometries for specific functions. Traditionally, the main ceramic 3D printing technologies consist of a suspension of powder in organic polymers thus constituting an organic-inorganic hybrid, which after polymerization will undergo a ceramization process during heat treatment.[18] Usually the polymer mixture consists in a blend of different highly acrylated photoactive monomers, for example, mixtures of di-functional (meth)acrylate with tri- or tetra functional (meth)acrylates. However, the low stability of powder dispersion and the sedimentation during 3D printing makes the printed object inhomogeneous and full of defects.[19,20] The polymeric nature of the preceramic precursor opens the door to easy and straightforward AM of ceramics. Indeed, PDCs can be tuned "on-demand" by chemical modification such as grafting on the precursor's backbone making the latter directly printable.

Thermoplastic moieties grafted on preceramic polymers or the preceramic polymer itself can be printed by fused deposition modeling.[21–23] This process relies on the polymer fusion during deposition followed by the drying of the polymer leading to a solidified object. This AM technique has been used to elaborate complex non oxide ceramic 3D structures such as honeycombs by printing a polymer template and impregnating it with a liquid preceramic resin as most of the Si-based preceramic polymers exhibit a high glass transition temperature.[21] However, objects with high anisotropy are produced, and therefore defects and random porosities can be present in the final ceramics.[20] A more accurate AM technique, based on the photopolymerization of preceramic polymers, can be employed to fabricate defect-free, near-net shape objects with a precise control of the amount, shape and direction of pores. The photopolymerization occurs mostly with certain types of monomers such as acrylate and methacrylate. These monomers will undergo rapid photopolymerization under ultraviolet (UV) light in presence of a photoinitiator (PI). The PI will be cleaved under UV light generating a radical, which will initiate the polymerization process between C = C of two monomers. However, free radical polymerization is severely inhibited by oxygen, which leads to numerous defects in photopolymerized polymers such as low conversion, slow rates, low curing depth, and sticky surfaces. In order to overcome these issues, two approaches can be used: (1) modifying the processing parameters, such as higher PI concentration or higher light intensities or (2) modifying the composition of the polymer mixture.[24] Some polymer systems are well known to overcome oxygen inhibition, particularly the thiol-ene chemistry, which is not oxygen sensitive, does not require a high amount of PI, and leads to high curing speed and good surface/depth.[25] It also allows the elaboration of high Tg polymers for high performances.[26] Thiol-ene photopolymerization relies on the radical click-reaction between C = C bond and radical activated thiol compounds. Therefore, it has been applied to materials science for high-end applications.[27,28] It has also been applied to prepare precursors for silicon-based ceramics.[29,30] Several AM technologies are based on photopolymerization where a liquid photopolymer in a vat is selectively cured by UV-activated polymerization, for example, stereolithography (SLA), digital light processing (DLP) or UV-liquid crystal display (UV-LCD). In a typical UV-3D printing process, a 3D computer aided design (CAD) is displayed on the UV-LCD screen, or patterned with UV light in case of SLA and DLP. During the printing process, UV light at 405 nm passes through a transparent fluoropolymer film to reach the resin tank and start the polymerization. Layers are deposited onto an aluminum platform that goes up down in the resin vat.[31] To be directly cured by light polymerization, preceramic polymers need to be photoactive. The photoactivity of polymers can be determined by means of fourier transform infrared spectroscopy (FTIR)-attenuated total reflection (ATR) spectroscopy and photo differential scanning calorimetry (Photo DSC).[32–34] The grafting of a photoactive moiety onto a preceramic polymer backbone was first reported by Thorne et al. in 1994 for the fabrication of SiC from UV curable polycarbosilane.[35] This technique can be used for the fabrication of SiOC or SiCN ceramics.[36,37] The presence of functional groups such as amino -NH, hydroxy -OH and alkoxy -OR moieties on the preceramic polymer (e.g., polysilazanes, polysiloxanes) allows facile grafting of the photoactive functions. After 3D printing of the desired object, and during pyrolysis,

the polymer-to-ceramic transformation takes place and is accompanied by object shrinkage and mass loss.[38] This mass loss is described as the ceramic yield. Pure preceramic resins are widely chosen due to their high ceramic yield.[39,40] The modification of the inorganic polymers with organic moieties will significantly decrease the ceramic yield. Indeed, during pyrolysis organic residues will be evacuated as low molecular weight hydrocarbons and gases such as methane, hydrogen, carbon dioxide, and many other gases depending on the chemical composition of the preceramic polymer.

UV-based AM techniques are the best choice to obtain complex 3D structures for many applications such as automotive parts that need high resistance, membranes, and electrodes for energy and environmental applications, bone/dental implants… Moreover, photopolymerization can be used in two photon photopolymerization in order to make micrometer to nanometer scaled objects. This technique is widely used in microelectromechanical systems[41] and micro biomedical devices.[42] Finally, 3D ceramic complex structures are used as catalyst supports for many industrial applications. A metallic-based catalyst (Pd, Pt, Ni…) can be immobilized on the surface of a robust ceramic through surface organometallic chemistry.[43] Another promising approach consists in direct molecular modification of the preceramic polymer and selective incorporation of the metal in the polymeric backbone.[44] The manufacturing of complex 3D structures through 3D printing can lead to highly active and selective catalysts.[45]

In this work, we focused on the design and fabrication of silicon oxycarbide (SiOC) with 3D cellular structures. The additive manufacturing technique that we selected is UV-LCD based on vat photopolymerization. A commercially available SiOC precursor (i.e., SILRES MK methyl silsesquioxane with a ceramic yield close to 80%[40]) was chemically modified according to two approaches in order to introduce photopolymerizable ends. Three organic photoactive moieties were investigated: 1,6-hexanediol diacrylate, trimethoxysilylpropylmethacrylate and vinyltrimethoxysilane/1,6-hexandithiol blend. Differently from previous literature, a monoacrylated source precursor is unveiled to decrease the amount of organic molecules while ensuring a high efficiency of polymerization, shape retention, and good yield upon pyrolysis. The polymer-to-ceramic transformation was performed slowly to deliver defect-free ceramics while achieving good surface quality and dimensional precision. Microscopy techniques were used to determine the surface aspect and the defects of each sample.

The versatile production of 3D SiOC geometries through facile UV 3D printing paves the way to mass fabrication of high performance ceramics with complex 3D structures for technological, environmental, and biomedical applications.

2 | EXPERIMENTAL PROCEDURES

2.1 | Materials

The preceramic polymer used in this work is a methyl-silsesquioxane resin powder (SILRES MK, Wacker-Chemie GmbH) precursor of SiOC. Photoactive moieties grafted on the resin are trimethoxysilylpropylmethacrylate (TMSPM, Sigma Aldrich), vinyltrimethoxysilane (VTMS, Sigma Aldrich). Monomers used as co-reagents for photopolymerization are 1,6-hexandioldiacrylate (HDDA, Sigma Aldrich) and 1,6-hexanedithiol (HDT, TCI Chemicals). Diphenyl(2,4,6-trimethylbenzoyl)phosphine oxide (TPO, Sigma Aldrich) was used as polymerization PI under UV-light. Genorad 16 (Rahn AG) was used as radical polymerization inhibitor for controlled photopolymerization. Tripropylene glycol monomethyl ether (TPM, Sigma Aldrich) was used as solvent. All chemicals were used without further purification. The pyrolysis was conducted under argon (99.999%) (Ar, Linde).

Photopolymer preceramic resins were synthesized according to Zanchetta et al.[36]: in a dry flask 5 g of SILRES MK was added and dissolved in 5 ml TPM under stirring. Using sonication for 10 min can help dissolving the resin. Once the resin is dissolved, 5 ml of TMSPM or VTMS was added with a syringe. In order to induce the sol-gel process for grafting of the TMSPM or VTMS, 200 μl of 2 M HCl were added with a 200 μl micropipette. The reaction time was set to 12 h under magnetic stirring at room temperature. After 12 h the photoactive preceramic polymers were obtained.

Formulation of the SIRLES MK+TMSPM photopolymerizable resin for UV induced 3D printing was prepared as follows: the obtained sol-gel photopolymerizable resin was mixed with 3 wt% diphenyl(2,4,6-trimethylbenzoyl)phosphine oxide (TPO) powder and Genorad 16.

Formulation of the SILRES MK+VTMS photopolymerizable resin for UV induced 3D printing was prepared as follows: the obtained sol-gel photopolymerizable resin was mixed with 1,6-hexanedithiol, in order to promote the thiol-ene photopolymerization by reaction between its -SH groups and the alkene moieties of the vinyltrimethoxysilane. Diphenyl(2,4,6-trimethylbenzoyl)phosphine oxide (TPO) powder (3 wt%) and Genorad 16 were added.

Formulation of the SILRES MK+HDDA resin was prepared by blending the two components with diphenyl(2,4,6-trimethylbenzoyl)phosphine oxide (TPO) powder (3 wt%) and Genorad 16.

All formulations were prepared and stored in aluminum foil covered flasks in order to avoid any reaction induced by direct light (sunlight or artificial light).

The photopolymerization process will take place through the dissociation of TPO under UV radiations leading to free radicals. Genorad 16 will inhibit the background photopolymerization and avoid edge-effects on the printed objects.

2.2 | UV-LCD 3D printing

3D printing of preceramic polymers was conducted on a Phrozen Sonic Mini 4K (Phrozen, Taiwan) printer based on UV-LCD technology. The UV light was provided by a 405 nm 4K UV-LCD screen with a light intensity of 2.5 mW/cm^2. The xy-axis resolution is 35 μm. The layer thickness resolution is set between .01 and .30 mm and determined when designing the 3D-CAD system. Every centimeter sized object could be printed in about 45 min. All the printing parameters are presented in the Results and Discussion section. All objects were post-treated for 60 min using a UV curing chamber (CB-5230, CUREbox, USA) for a complete conversion of the photopolymers.

2.3 | Polymer-to-ceramic transformation

The polymer-to-ceramic transformation was achieved by thermal treatment of the printed parts in a tubular furnace (type ROS20/250/12 with a silica tube, Thermconcept, Germany) under argon. The pyrolysis temperature was set to 1000°C with a slow heating rate (1°C/min) and dwelling time of 2 h to avoid voids and cracks formation while completely converting the polymers into ceramics.

Figure SI 1 summarizes the different fabrication steps of 3D printed SiOC ceramics.

2.4 | Characterizations

Thermogravimetric analysis of all polymers was performed on a TGA-SDT Q600 thermal analysis device (TA Instruments, USA) at atmospheric pressure. The heating rate was fixed at 5°C/min to 1000°C under inert atmosphere. The chemical structure of the preceramic polymers was determined by Fourier Transform Infrared spectroscopy with a FTIR Nexus spectrometer (ThermoFisher Scientific, USA) using ATR mode in the range of 500–4000 cm^{-1}. The photopolymerizability and conversion of the samples was characterized using photo-differential scanning calorimetry (DSC1 calorimetric differential analyzer, METTLER TOLEDO, Switzerland equipped with a UV lamp: wavelength 405 nm, 127.11 mW.cm^{-2} at 100% light intensity). The morphology of pyrolyzed 3D structures was observed by the super depth field three-dimensional optical microscope (VHX-7000, KEYENCE, Japan) and scanning electron microscopy (SEM) (Hitachi S4800, Hitachi High-Tech Corporation, Japan, operating with an acceleration voltage of 2 kV). The chemical composition of SiOC 3D ceramics was analyzed using energy dispersive X-ray spectroscopy (Detector: Oxford Instruments X-Max AZTEC, UK; Microscopy: Zeiss EVO HD15, Germany).

3 | RESULTS AND DISCUSSIONS

3.1 | Synthesis and characterization of photocurable preceramic polymers

Different classes of monomers were introduced in the precursor's backbone and evaluated to be readily photopolymerized under UV light. We describe two approaches for the manufacturing of SiOC ceramics through UV-LCD: the first one is the blending of preceramic silicone resin with a photoactive monomer. The second one is the synthesis of single source photopolymers precursors of SiOC.

The first approach is based on the mixing of 1,6-hexanediol diacrylate (HDDA) with the silicon resin. The preceramic resin is readily mixed in equal parts with an acrylate monomer. The acrylate monomers will undergo polymerization when exposed to UV light in presence of a PI and encapsulate the preceramic resin (SILRES MK) in the crosslinked polymer (See mechanism in Figure SI 2). The system that results from this approach is called HDDA m-SILRES ("m" standing for modified).

The second approach to obtain a photopolymer is the grafting of photoactive moieties onto the methylsilsesquioxane backbone. Two different photoactive monomers were grafted and their reactivity compared. The first monomer is trimethoxysilylpropylmethacrylate (TMSPM), and the second one is VTMS. The grafting is obtained through a sol-gel acid catalyzed reaction between the silanol/alkoxysilane groups of the resin and the methoxysilane groups of the monomer.[36] The systems are named TMSPM m-SILRES and VTMS m-SILRES ("m" standing for modified), respectively.

Photopolymerization of photoactive moieties is possible in the presence of a PI, TPO. Under UV light, it will cleave and lead to the formation of radicals. Figure SI 2 shows the mechanism in the case of HDDA and Figure SI 3 in the case of TMSPM. The radicals will react with the C = C bonds leading to propagation of a polymeric chain, through radical polymerization of olefin-based monomers, and therefore to crosslinking. It will either encapsulate the preceramic resin, for HDDA (Figure 1A), or it will lead to a crosslinked system with the preceramic resin as an integral part of the polymer backbone (Figure 1B). For VTMS, the vinyl group itself is not

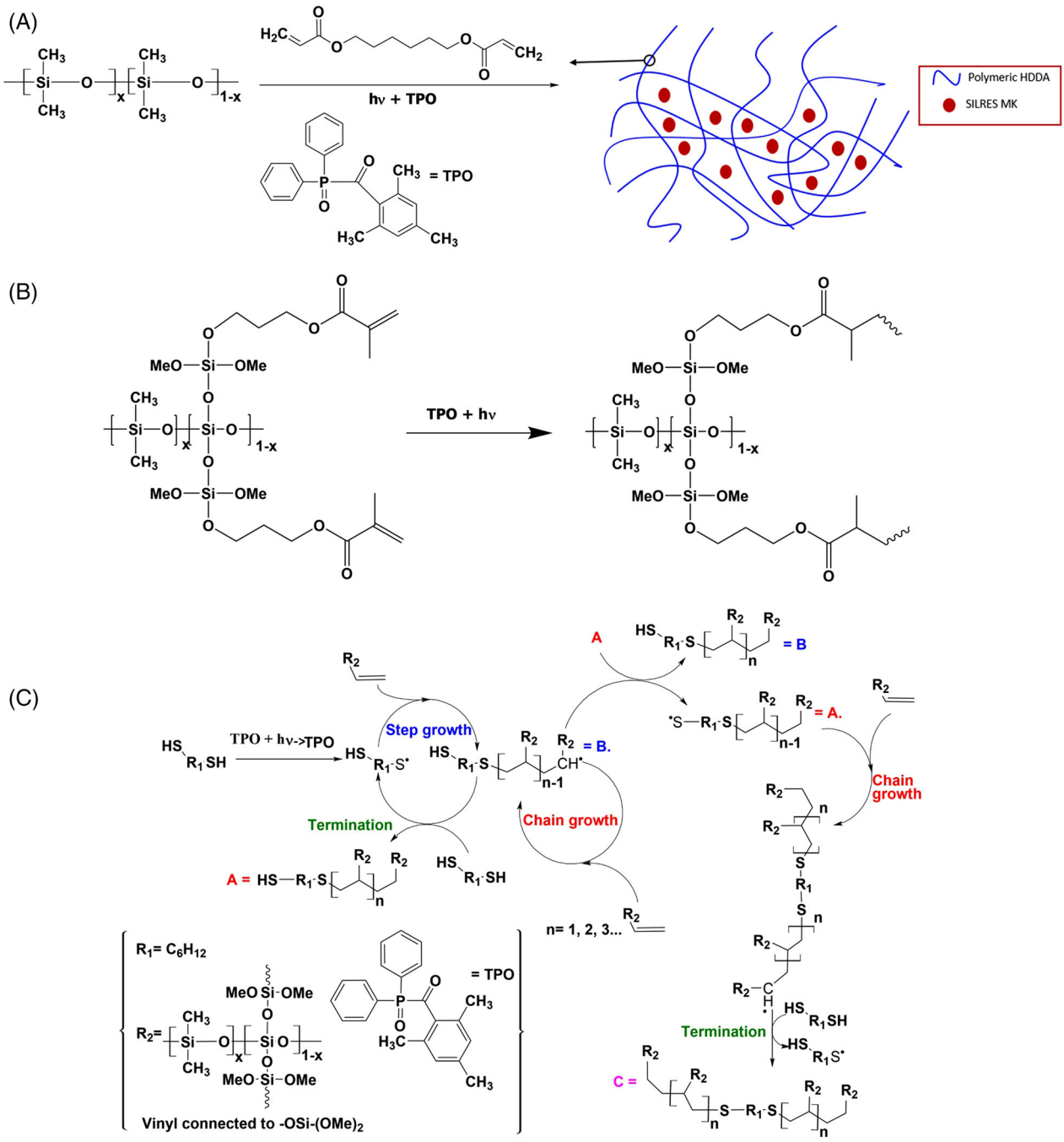

FIGURE 1 (A) HDDA m-SILRES photopolymerization, (B) trimethoxysilylpropylmethacrylate (TMSPM) m-SILRES photpolymerization, and (C) vinyltrimethoxysilane (VTMS) m-SILRES thiol-ene mediated photpolymerization

photoactive. Therefore, we considered a thiol-ene photo-click reaction, the vinyl moiety grafted will react with -SH groups of 1,6-hexanedithiol (HDT) leading to a thioether linkage. As shown in Figure 1C, the polymerization occurs as follows: the thiol monomer is radically activated by TPO and initiates a radical polymerization of the vinyl moiety giving B●. Then the chain growth takes place by two different routes: propagation of the olefin backbone leading to A after termination and radical initiation of A to give A● that will initiate crosslinking between two polymerized olefin-type backbones and results in C. In the polymer mixture three major components will coexist together A, B, and C in a highly crosslinked form.

We monitored the photopolymerization reaction using FTIR-ATR spectroscopy. For acrylate/methacrylate-based systems, the evolution of the intensity of the band at 1636 cm^{-1} (C = C stretch associated with acrylate/methacrylate) is key to prove the photopolymerization. As shown in Figure 2, the C = C band drastically decreases upon exposure to light suggesting thus that the

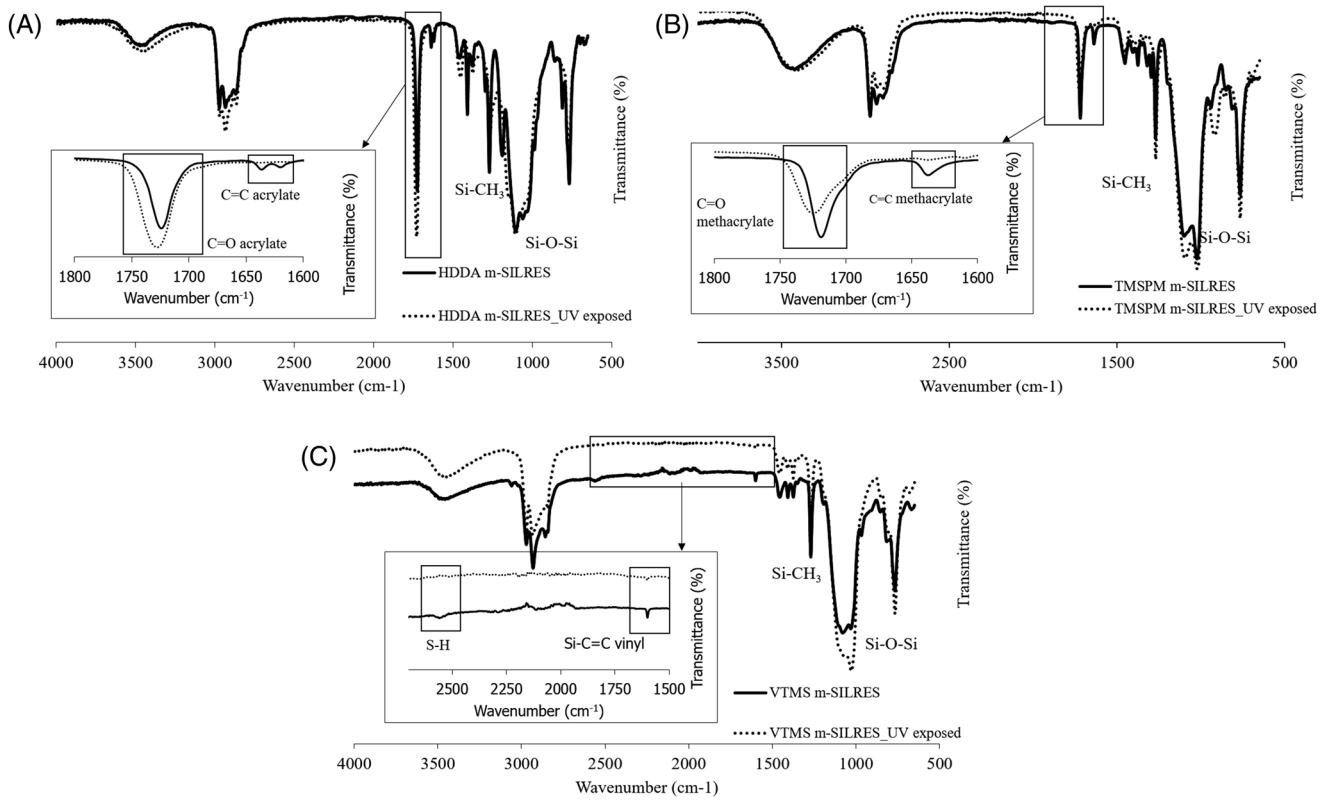

FIGURE 2 FTIR-attenuated total reflection (ATR) curves before (plain line) and after (dotted line) UV exposure (A) HDDA m-SILRES, (B) trimethoxysilylpropylmethacrylate (TMSPM) m-SILRES, and (C) vinyltrimethoxysilane (VTMS) m-SILRES

acrylate/methacrylate units have crosslinked. As for the thiol-ene photo-click system, the focus is on the band at 1599 cm^{-1} (C = C stretch associated with vinyl groups). The thiols band around 2578 cm^{-1} should be considered to see the evolution of the crosslinking, but the weak absorption of -SH under Infrared makes it difficult to identify the thiol-ene reaction[29]; therefore we will only consider the evolution of C = C band for the vinyl groups.

To further characterize the photopolymerization behavior, we used the photo-differential scanning calorimetry (Photo-DSC), which is a powerful tool based on real time differential scanning calorimetry under UV-irradiation. As polymerization reactions are known to be exothermic, all exotherm peaks were considered in order to compare the reactivity of each system. As shown in Figure 3, all three systems exhibit strong exotherm peaks directly after UV exposure. The presence of an exotherm in a photocurable system depicts a high curing efficiency within seconds. Additionally, a UV dose study has been conducted in order to compare the effective photopolymerizability of the preceramic polymer systems under different light intensities. In order to conduct the UV dose study, each sample was exposed to UV light, and the corresponding thermogram was recorded using DSC. The UV lamp used was set up to 25%, 50%, and 100% light intensity corresponding, respectively, to 30.27 mW/cm^2, 60.84 mW/cm^2, and 127.11 mW/cm^2. As we can see on the corresponding thermogram, for each system the evolution of the polymerization exothermic peak is a function of the UV light intensity. For every system when the intensity increases, the polymerization enthalpy associated with the exotherm increases, and the conversion rate is higher for higher intensity. We observe in Figure 3A a slight difference of conversion rate at 100% light intensity versus 50% intensity. As we can see, even the lowest intensity induces a 50% rate photopolymerization in less than 10 s. This means that, even if the light intensity of the UV-LCD screen is lower than that of 3D printing of polymer systems, additive manufacturing of preceramic polymers via UV-LCD is possible.

The curing ability of each system can be compared using normalized integral of the exotherm. Considering a time frame of 8–10 s, each system can be effectively cured at 50% conversion.[29] This consideration confirms that our systems can be used in vat photopolymerization AM. Indeed, UV-LCD 3D printing needs fast and efficient photopolymerization. TMSPM m-SILRES is the system, which has the lowest exotherm peak and lowest efficient conversion among all three systems. This can be explained by the lower reactivity of methacrylate functional groups

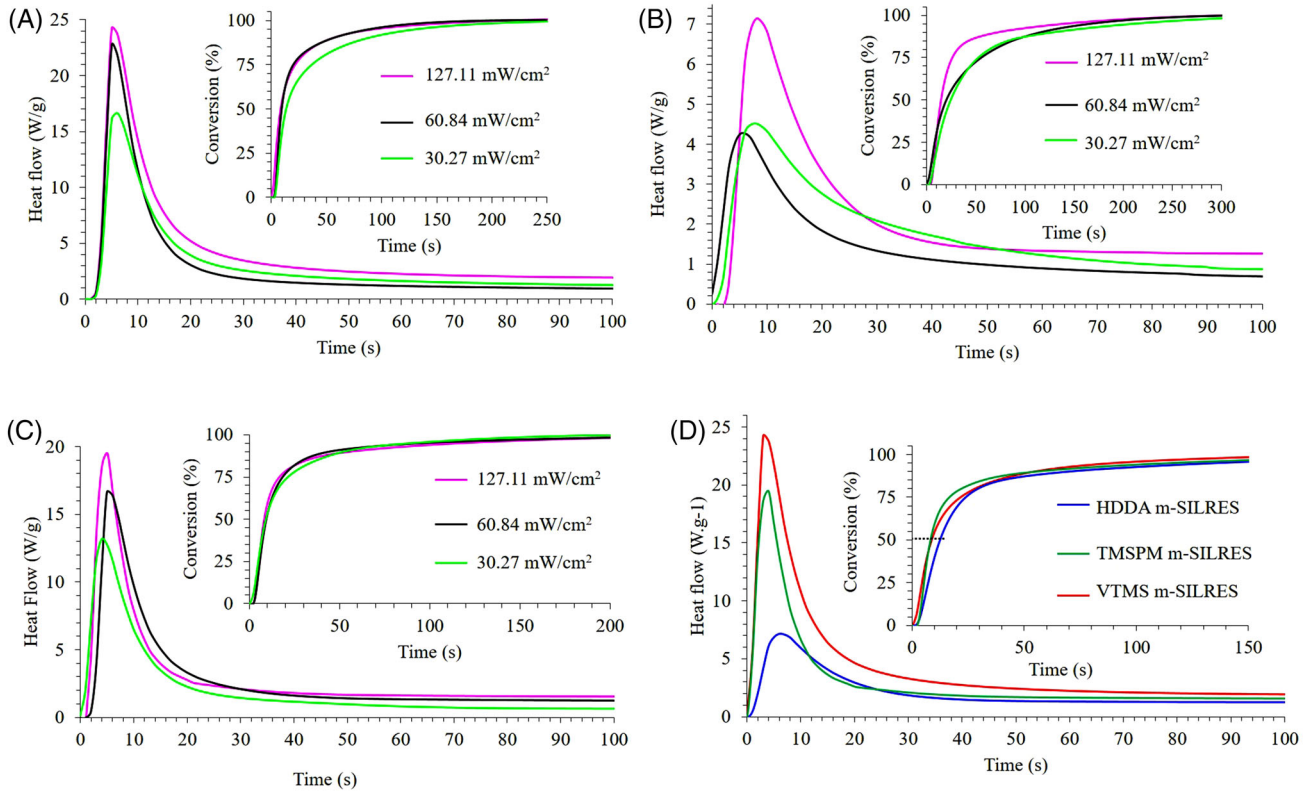

FIGURE 3 Photo-differential scanning calorimetry (DSC) curves of photocurable preceramic resins and their derived conversion curves as inset (A) HDDA m-SILRES, (B) trimethoxysilylpropylmethacrylate (TMSPM) m-SILRES, (C) vinyltrimethoxysilane (VTMS) m-SILRES, and (D) comparison of the three systems, that is, HDAA m-SILRES, TMSPM m-SILRES, VTMS m-SILRES

compared to acrylate and thiol-ene groups. Methacrylate has a slower radical photopolymerization due to the presence of a methyl group, which slightly inhibits the formation of radicals. Acrylate in HDDA m-SILRES systems allows the formation of radicals, and therefore the curing efficiency is higher when compared to methacrylate. Finally, the last system VTMS m-SILRES is based on thiol-ene click photopolymerization. This system has the highest curing efficiency among the three systems. Nevertheless, even if the described systems have different curing rates they can all be applied to UV-LCD 3D printing. The physical state related to the crosslinking density of the printed polymer will have a significant effect on the polymer-to-ceramic transformation discussed below. HDDA m-SILRES has the lowest crosslinking density. The object obtained is soft, rubbery and sticky reflecting the low crosslinking density, and the oxygen inhibition of the photopolymerization process. A postcure treatment was then applied to enhance the crosslinking density. On another hand, TMSPM m-SILRES gives hard brittle Plexiglas-like object. TMSPM m-SILRES 3D materials are sensitive to light even after curing leading to fractured pieces when exposed. Therefore, no post-treatment under UV light was conducted for TMSPM m-SILRES. Finally, even if VTMS m-SILRES printed material is a hard and highly crosslinked polymer, it has not the brittleness of the TMSPM m-SILRES. Through the postcure treatment, the object changed from colorless-translucent to opaque-yellowish representing a highly crosslinked system.

3.2 | Polymer-to-ceramic transformation

In order to obtain ceramic objects, the printed parts have undergone the same treatment. After printing, each part is washed with isopropanol to remove any unreacted resin, then dried with compressed air, and postcured using a UV-chamber. Postcure time has been set at 60 min for each object to maximize the photopolymerization and to have an object that will maintain its shape evenly throughout pyrolysis. After postcure, the printed pieces were measured, weighed, and placed into alumina crucible for pyrolysis under Ar flow. The thermal treatment program was defined using thermogravimetric analysis (TGA) in order to predict the evolution of the system with temperature. As shown in Figure 4, we can compare the thermal evolution of each printed object with its respective components and with each other. For every system, we observe three main steps during thermal treatment:

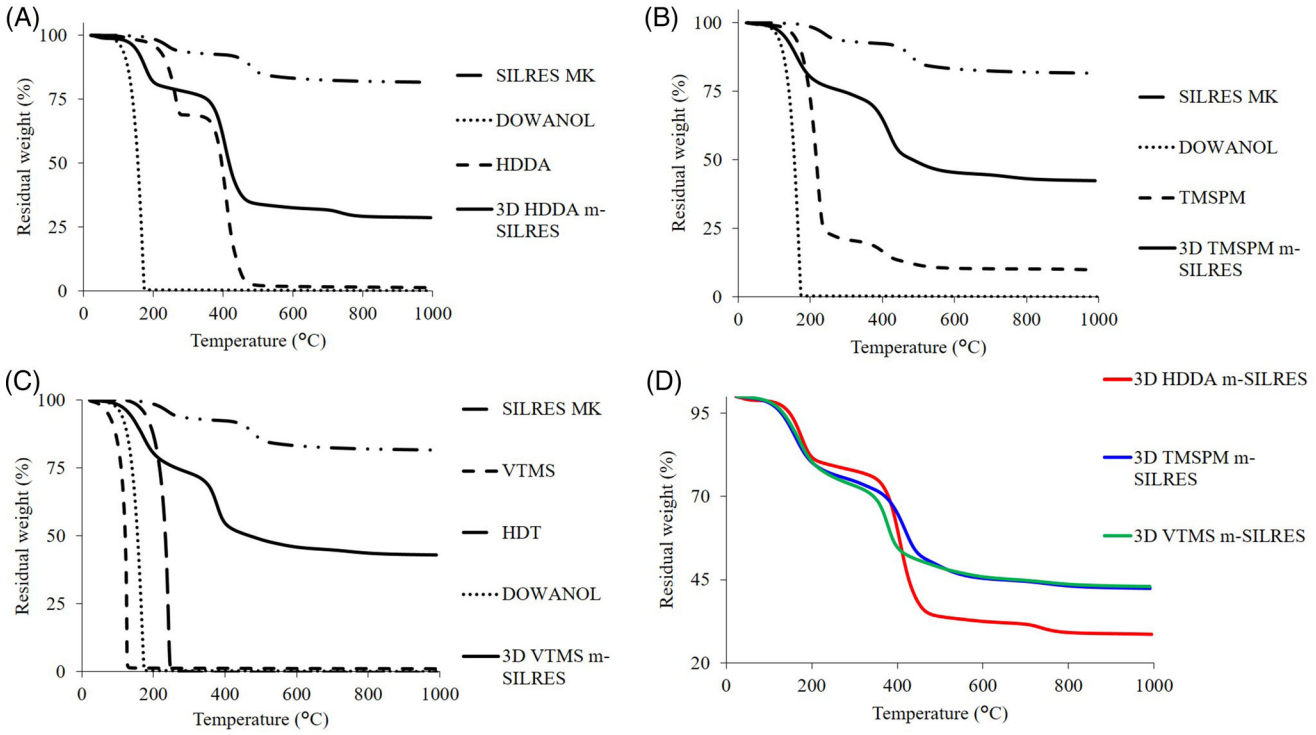

FIGURE 4 TGA curves under inert atmopshere of (A) HDDA m-SILRES, (B) trimethoxysilylpropylmethacrylate (TMSPM) m-SILRES, (C) vinyltrimethoxysilane (VTMS) m-SILRES, and (D) systems comparison

TABLE 1 Ceramic yield determination through TGA analysis

3D printed green body	Ceramic yield (%)
HDDA m-SILRES	29
TMSPM m-SILRES	42
VTMS m-SILRES	43

Abbreviations: TMSPM, trimethoxysilylpropylmethacrylate; VTMS, vinyltrimethoxysilane.

from 25 to 200°C, 200 to 400°C, and 400 to 1000°C. Each step is associated with gaseous volatile compounds contained in the organic parts of the hybrid polymers. The first weight loss between 25 and 200°C is related to the evaporation of residual water and TPM. The second one between 200°C and 400°C translates the degradation of the organic parts of SILRES MK and the different additives (TMSPM, HDDA, VTMS-HDT). Finally, the third weight loss between 400 and 1000°C step corresponds to the release of hydrogen and methane gases during SILRES MK ceramization. Mass loss and volume shrinkage always accompany the ceramization. The volume shrinkage and mass loss can be reduced with highly crosslinked systems; indeed the crosslinking density will reduce the volatilization of the fragments cleaved during pyrolysis. The ceramic yield, determined by means of TGA (Figure 4), is directly correlated to the amount of organic compounds in the resin. As shown in Table 1, HDDA m-SILRES system has the lowest ceramic yield (29%) compared to the other systems. This is probably related to the amount of organic compounds in HDDA, which is higher than that of VTMS-HDT and TMSPM exhibiting 43% and 42% ceramic yields, respectively. Another approach to decrease the weight loss and volume shrinkage is the addition of fillers,[46] but this was beyond the scope of this work where only UV curing was considered without the aid of fillers.

3.3 | Morphological characterization

For every system, a black SiOC 3D ceramic can be obtained as a dense or macroporous monolith. Pyrolysis of porous 3D printed objects leads to SiOC ceramics without macroscopic defects, whereas massive discs (not shown here) embed cracks and fractures. This difference between porous and dense objects can be explained with the means of escape for gases.[29] Indeed, porous structures or small dense parts are the best options for avoiding residual pores and cracks caused by the polymer decomposition during pyrolysis.[47] Defect-free objects are easily obtained by having features of less than 2 mm in at least one direction reducing the diffusion pathways of gases in the walls. Thus monolithic compounds, which had higher dimensions, could not be obtained without defects. The porous

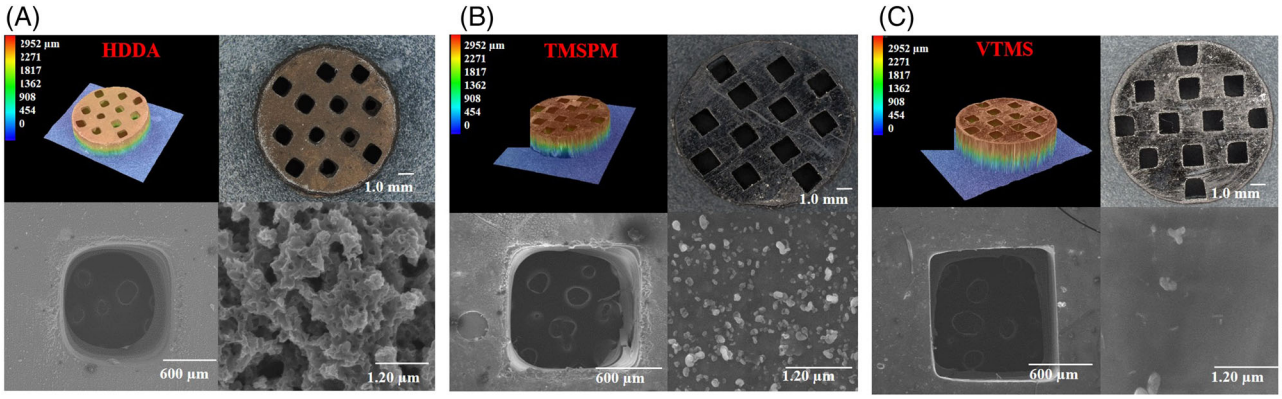

FIGURE 5 (A) HDDA m-SILRES, (B) trimethoxysilylpropylmethacrylate (TMSPM) m-SILRES, and (C) vinyltrimethoxysilane (VTMS) m-SILRES. For each system from left to right: - first row: 3D view of pyrolyzed porous ceramics/microscopy - second row: SEM microscopy of the pores at 600 μm/surface SEM at 1.20 μm

objects were crack-free, thanks to the open pores in the CAD design. The visual aspect of the ceramic evolves from lustrous to matte. The most crosslinked system VTMS m-SILRES was the most lustrous and presented the best resolution, while the least crosslinked system, HDDA m-SIRLES, was matte. The resolution of the open pores of the porous object was not as good as the VTMS m-SILRES, but the dense part was crack and defect-free. Similarly, we produced crack-free porous printed part with TMSPM m-SILRES.

As shown in Figure 5, the resolution of the printed parts differs for each sample. The resolution on the square pore of HDDA m-SILRES is lower because edge effects occurred during photopolymerization. UV light was scattered around the pattern and lead to a rounding of the pore. In the second system TMSPM m-SILRES, the surface resolution of the pore was good with a faithful reproduction of the CAD design. However, in the depth of the structure, we can see edges effects, which even Genorad 16 could not inhibit.

Finally, the most accurate resolutiofn was obtained with VTMS m-SILRES system. As we can see in Figure 5, the square shape of the pore magnified at 600 μm was almost preserved. We can correlate these considerations with the crosslinking density of the polymer systems. The higher the crosslinking density the higher the resolution. Looking at SEM pictures, at 1.20 μm magnification, we can observe differences in the surface conditions of each system. 3D HDDA m-SILRES has a rough, porous-like surface compared to 3D TMSPM m-SILRES and 3D VTMS m-SILRES. These two systems have a relatively smoother surface than that of 3D HDDA m-SILRES. Rugosity measurements were conducted on the surface of each sample. As shown is Table 2, we can see that the average arithmetic rugosity Ra is more than three times higher for 3D HDDA m-SILRES than 3D VTMS m-SILRES. The rugosity of 3D TMSPM m-SILRES is higher than that of 3D VTMS m-SILRES but

TABLE 2 Rugosity measurements for each system (Ra for average arithmetic rugosity/Rz for surface rugosity)

3D printed ceramic	Ra (μm)	Rz (μm)
HDDA m-SILRES	50.3175	228.145
TMSPM m-SILRES	30.42	127.495
VTMS m-SILRES	17.9725	86.335

Abbreviations: TMSPM, trimethoxysilylpropylmethacrylate; VTMS, vinyltrimethoxysilane.

in accordance with SEM images lower than 3D HDDA m-SILRES.

In addition to the mass loss, volume shrinkage could be observed on each sample. Indeed, mass loss and shrinkage of preceramic resins upon pyrolysis are correlated and both can be tuned by crosslinking of the initial resin. HDDA m-SILRES has a volume shrinkage of 73%, whereas TMPSM m-SILRES and VTMS m-SILRES were obtained with a volume shrinkage of respectively 74.5% and 75%. Even though the volume shrinkage is quite high for the three systems, but it is linear, uniform, and isotropic, which does not cause any deformation of the 3D structure.

In addition to these analyses, 3D microscopy confirms the shape retention of the 3D objects after pyrolysis. Proportions between the size of the disc and the pores stay the same as before pyrolysis. Moreover, the surface is leveled, as the orange color distribution on the surface is homogeneous.

To study the surface composition of every silicon oxycarbide object, energy-dispersive X-ray spectroscopy was used to get the elemental composition of the surface. For all three systems, we observe in Figure 6A homogenous surface distr of Si, O, C elements. The amount of each component of the ceramics is measured, and the mapping of each element shows a difference between each

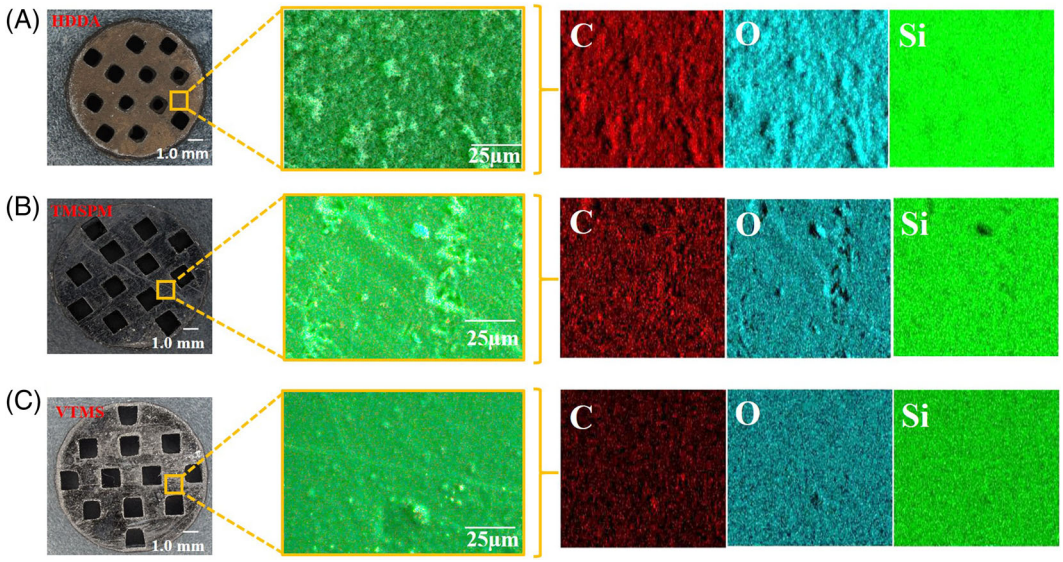

FIGURE 6 Energy-dispersive X-ray spectroscopy and elemental mapping of pyrolyzed ceramics (A) HDDA m-SILRES, (B) trimethoxysilylpropylmethacrylate (TMSPM) m-SILRES, and (C) vinyltrimethoxysilane (VTMS) m-SILRES

TABLE 3 Elemental composition of pyrolyzed samples under Ar at 1000°C

Preceramic resin	3D printed ceramic	Atomic composition (%)		
		Si	O	C
HDDA m-SILRES	$SiO_{1.62}C_{1.58}$	23.75	38.57	37.49
TMSPM m-SILRES	$SiO_{1.52}C_{1.1}$	27.54	41.78	30.41
VTMS m-SILRES	$SiO_{1.64}C_{0.85}$	28.53	46.95	24.32

Abbreviations: TMSPM, trimethoxysilylpropylmethacrylate; VTMS, vinyltrimethoxysilane.

system. 3D HDDA m-SILRES elemental mapping shows a high concentration of carbon whereas 3D TMSPM m-SILRES and 3D VTMS m-SILRES. The amount of oxygen looks almost the same for each system. Table 3 shows a normalization of the atomic repartition gives a ceramic system with the general formula SiO_xC_y, x and y determined with EDX atomic percentages. By normalizing the element silicon, we obtained ceramics with different stoichiometry. HDDA-based ceramic system leads to the most carbon-rich structure, whereas VTMS-based system has the lowest carbon content. This difference can be explained by the amount of carbon in the different precursors for each preceramic system.

4 | CONCLUSIONS

In this work, we were able to compare different approaches for the elaboration of photopolymers precursors of silicon oxycarbide for direct AM through vat photopolymerization. The first approach developed is based on the formulation of a single source of acrylate, 1,6-hexanediol diacrylate (HDDA) by direct blending of the silsesquioxane resin with the HDDA and TPO. The second approach consisted in grafting two distinct photopolymerizable groups: trimethoxysilylpropylmethacrylate (TMSPM) and vinyltrimethoxysilane (VTMS) by acid catalyzed sol-gel grafting of the photoactive moieties. The three resins were printed using a UV-LCD printer. UV-LCD printability was proved using photo differential scanning calorimetry. Each system exhibited a sharp exotherm peak with the lowest reactivity for the methacrylate-based system (TMSPM m-SILRES). After printing, the VTMS-based system had the highest resolution. HDDA m-SILRES presented the highest rugosity and non dense surface, whereas the TMSPM m-SIRLES had a less rough surface. We can suggest that the higher the crosslinking the higher the density. Indeed, there is less chain mobility and means of escape for the released gases during pyrolysis for a highly crosslinked system in comparison to a weakly crosslinked system where the chains can be easily cleaved. Finally, the elemental analysis of each system with EDX allows us to determine the stoichiometry, which is in agreement with the nature of the organic additive used for UV-curing. Therefore, by tuning the nature of the organic additive, we can design precisely the amount of amorphous carbon. These approaches represent an easy, scalable, and energy-efficient process for fabricating complex 3D SiOC structures for many applications requiring highly resistant materials with precise shapes.

In this work, we focused on SiOC structures, but other ceramic compositions can be produced by this versatile

approach. Moreover, porous and dense ceramic structures are expected to be printed; however some technical issues are inevitably encountered when printing dense objects, which is reflected by the occurrence of fractures and cracks upon pyrolysis. In order to overcome some of these technical issues future work will consist of adding active or passive fillers acting as aiding agents and in optimizing the thermal treatments. We are working as well on processing non oxide 3D ceramics, which are particularly interesting for high-temperature applications.

ACKNOWLEDGMENT

Chrystelle Salameh acknowledges the French National Agency (ANR) that funded this work under the JCJC program MONOME-ANR-20-CE08-0009.

FUNDING INFORMATION

French National Agency (ANR), Grant Number: ANR-20-CE08-0009

CONFLICT OF INTEREST

The authors declare that there is no conflict of interest that could be perceived as prejudicing the impartiality of the research reported.

ORCID

Chrystelle Salameh https://orcid.org/0000-0002-8188-6637

REFERENCES

1. Riedel R, Mera G, Hauser R, Klonczynski A. Silicon-based polymer-derived ceramics: synthesis properties and applications-a review: dedicated to Prof. Dr. Fritz Aldinger on the occasion of his 65th birthday. J Ceram Soc Jpn. 2006;114(1330):425–44.
2. Burger W, Kiefer G. Alumina, zirconia and their composite ceramics with properties tailored for medical applications. J Compos Sci. 2021;5(11):306.
3. Song SY, Park MS, Lee D, Lee JW, Yun JS. Optimization and characterization of high-viscosity ZrO2 ceramic nanocomposite resins for supportless stereolithography. Mater Des. 2019;180:107960.
4. Nikas V, Gallis S, Huang M, Kaloyeros AE, Nguyen APD, Stesmans A, et al. The origin of white luminescence from silicon oxycarbide thin films. Appl Phys Lett. 2014;104(6):061906.
5. Zhang Y, Quaranta A, Domenico Soraru G. Synthesis and luminescent properties of novel Eu2+-doped silicon oxycarbide glasses. Opt Mater. 2004;24(4):601–5.
6. Sorarù GD, Modena S, Bettotti P, Das G, Mariotto G, Pavesi L. Si nanocrystals obtained through polymer pyrolysis. Appl Phys Lett. 2003;83(4):749–51.
7. Dibandjo P, Diré S, Babonneau F, Soraru GD. Influence of the polymer architecture on the high temperature behavior of SiCO glasses: a comparison between linear- and cyclic-derived precursors. J Non-Cryst Solids. 2010;356(3):132–40.
8. Bréquel H, Parmentier J, Walter S, Badheka R, Trimmel G, Masse S, et al. Systematic structural characterization of the high-temperature behavior of nearly stoichiometric silicon oxycarbide glasses. Chem Mater. 2004;16(13):2585–98.
9. Sorarù GD, Tavonatti C, Kundanati L, Pugno N, Biesuz M. Effect of the pyrolysis atmosphere on the mechanical properties of polymer-derived SiOC and SiCN. J Am Ceram Soc. 2020;103(11):6519–30.
10. Sorarù GD, Modena S, Guadagnino E, Colombo P, Egan J, Pantano C. Chemical Durability of Silicon Oxycarbide Glasses. J Am Ceram Soc. 2002;85(6):1529–36.
11. Krasnyi BL, Tarasovskii VP, Rakhmanova EV, Bondar' VV. Chemical resistance of ceramic materials in acids and alkalis. Glass Ceram. 2004;61(9/10):337–9.
12. Salameh C, Bruma A, Malo S, Demirci UB, Miele P, Bernard S. Monodisperse platinum nanoparticles supported on highly ordered mesoporous silicon nitride nanoblocks: superior catalytic activity for hydrogen generation from sodium borohydride. RSC Adv. 2015;5(72):58943–51.
13. Salameh C, Moussa G, Bruma A, Fantozzi G, Malo S, Miele P, et al. Robust 3D boron nitride nanoscaffolds for remarkable hydrogen storage capacity from ammonia borane. Energy Technol. 2018;6(3):570–7.
14. Mera G, Navrotsky A, Sen S, Kleebe HJ, Riedel R. Polymer-derived SiCN and SiOC ceramics – structure and energetics at the nanoscale. J Mater Chem A. 2013;1(12):3826.
15. Salameh C, Bernard S, Gervais C, Babonneau F, Bruma A, Malo S, et al. Chemistry of a series of aluminum-modified polysilazanes: synthesis, pyrolysis behaviour and microstructural evolution. J Eur Ceram Soc. 2019;39(2–3):183–94.
16. Hanniet Q, Boussmen M, Barés J, Huon V, Iatsunskyi I, Coy E, et al. Investigation of polymer-derived Si–(B)–C–N ceramic/reduced graphene oxide composite systems as active catalysts towards the hydrogen evolution reaction. Sci Rep. 2020;10(1):22003.
17. Colombo P, Mera G, Riedel R, Sorarù GD. Polymer-derived ceramics: 40 years of research and innovation in advanced ceramics: polymer-derived ceramics. J Am Ceram Soc. 2010. https://doi.org/10.1002/9783527631971.ch07
18. Li F, Ji X, Wu Z, Qi C, lai J, Xian Q, et al. Digital light processing 3D printing of ceramic shell for precision casting. Mater Lett. 2020;276:128037.
19. Eckel ZC, Zhou C, Martin JH, Jacobsen AJ, Carter WB, Schaedler TA. Additive manufacturing of polymer-derived ceramics. Science. 2016;351(6268):58–62.
20. Stansbury JW, Idacavage MJ. 3D printing with polymers: challenges among expanding options and opportunities. Dent Mater. 2016;32(1):54–64.
21. El Chawich G, El Hayek J, Rouessac V, Cot D, Rebière B, Habchi R, et al. Design and manufacturing of Si-based non-oxide cellular ceramic structures through indirect 3D printing. Materials. 2022;15(2):471.
22. Kulkarni A, Sorarù GD, Pearce JM. Polymer-derived SiOC replica of material extrusion-based 3-D printed plastics. Addit Manuf. 2020;32:100988.
23. Kulkarni A, Pearce J, Yang Y, Motta A, Sorarù GD. SiOC(N) cellular structures with dense struts by integrating fused filament fabrication 3D printing with polymer-derived ceramics. Adv Eng Mater. 2021;23(12):2100535.

24. Lee TY, Guymon CA, Jönsson ES, Hoyle CE. The effect of monomer structure on oxygen inhibition of (meth)acrylates photopolymerization. Polymer. 2004;45(18):6155–62.
25. Hoyle CE, Bowman CN. Thiol-ene click chemistry. Angew Chem Int Ed. 2010;49(9):1540–73.
26. Carioscia JA, Schneidewind L, O'Brien C, Ely R, Feeser C, Cramer N, et al. Thiol–norbornene materials: approaches to develop highTg thiol–ene polymers. J Polym Sci Part Polym Chem. 2007;45(23):5686–96.
27. Nair DP, Cramer NB, Scott TF, Bowman CN, Shandas R. Photopolymerized thiol-ene systems as shape memory polymers. Polymer. 2010;51(19):4383–9.
28. Li Q, Zhou H, Hoyle CE. The effect of thiol and ene structures on thiol–ene networks: photopolymerization, physical, mechanical and optical properties. Polymer. 2009;50(10):2237–45.
29. Wang X, Schmidt F, Hanaor D, Kamm PH, Li S, Gurlo A. Additive manufacturing of ceramics from preceramic polymers: a versatile stereolithographic approach assisted by thiol-ene click chemistry. Addit Manuf. 2019;27:80–90.
30. Obmann R, Schörpf S, Gorsche C, Liska R, Fey T, Konegger T. Porous polysilazane-derived ceramic structures generated through photopolymerization-assisted solidification templating. J Eur Ceram Soc. 2019;39(4):838–45.
31. Zakeri S, Vippola M, Levänen E. A comprehensive review of the photopolymerization of ceramic resins used in stereolithography. Addit Manuf. 2020;35:101177.
32. Gorsche C, Seidler K, Knaack P, Dorfinger P, Koch T, Stampfl J, et al. Rapid formation of regulated methacrylate networks yielding tough materials for lithography-based 3D printing. Polym Chem. 2016;7(11):2009–14.
33. Anseth KS, Wang CM, Bowman CN. Reaction behaviour and kinetic constants for photopolymerizations of multi(meth)acrylate monomers. Polymer. 1994;35(15):3243–50.
34. Bachmann J, Gleis E, Schmölzer S, Fruhmann G, Hinrichsen O. Photo-DSC method for liquid samples used in vat photopolymerization. Anal Chim Acta. 2021;1153:338268.
35. Thorne KJ, Johnson SE, Zheng H, Mackenzie JD, Hawthorne MF. Chemically designed, UV curable polycarbosilane polymer for the production of silicon carbide. Chem Mater. 1994;6(2):110–5.
36. Zanchetta E, Cattaldo M, Franchin G, Schwentenwein M, Homa J, Brusatin G, et al. Stereolithography of SiOC ceramic microcomponents. Adv Mater. 2016;28(2):370–6.
37. Li YH, Li XD, Kim DP. Acrylation of polyvinylsilazane with allyl bromide for an UV photosensitive inorganic polymer. J Organomet Chem. 2007;692(23):5303–6.
38. Schmidt J, Colombo P. Digital light processing of ceramic components from polysiloxanes. J Eur Ceram Soc. 2018;38(1):57–66.
39. Lavedrine A, Bahloul D, Goursat P, Choong Kwet Yive N, Corriu R, Leclerq D, et al. Pyrolysis of polyvinylsilazane precursors to silicon carbonitride. J Eur Ceram Soc. 1991;8(4):221–7.
40. Schelm K, Abreu Morales E, Scheffler M. Mechanical and surface-chemical properties of polymer derived ceramic replica foams. Materials. 2019;12(11):1870.
41. Park SH, Yang DY, Lee KS. Two-photon stereolithography for realizing ultraprecise three-dimensional nano/microdevices: two-photon stereolithography for nano/microdevices. Laser Photonics Rev. 2009;3(1–2):1–11.
42. Narayan RJ, Doraiswamy A, Chrisey DB, Chichkov BN. Medical prototyping using two photon polymerization. Mater Today. 2010;13(12):42–8.
43. Copéret C, Comas-Vives A, Conley MP, Estes DP, Fedorov A, Mougel V, et al. Surface organometallic and coordination chemistry toward single-site heterogeneous catalysts: strategies, methods, structures, and activities. Chem Rev. 2016;116(2):323–421.
44. Glatz G, Schmalz T, Kraus T, Haarmann F, Motz G, Kempe R. Copper-containing SiCN precursor ceramics (Cu@SiCN) as selective hydrocarbon oxidation catalysts using air as an oxidant. Chem - Eur J. 2010;16(14):4231–8.
45. Zhu J, Wu P, Chao Y, Yu J, Zhu W, Liu Z, et al. Recent advances in 3D printing for catalytic applications. Chem Eng J. 2022;433:134341.
46. Brinckmann SA, Patra N, Yao J, Ware TH, Frick CP, Fertig RS. Stereolithography of SiOC polymer-derived ceramics filled with SiC micronwhiskers. Adv Eng Mater. 2018;20(11):1800593.
47. Raj R, Pederiva L, Narisawa M, Soraru GD. On the onset of fracture as a silicon-based polymer converts into the ceramic phase. J Am Ceram Soc. 2019;102(3):924–9.

SUPPORTING INFORMATION

Additional supporting information can be found online in the Supporting Information section at the end of this article.

How to cite this article: Dory H, Miele P, Salameh C. UV-curable inorganic precursors enable direct 3D printing of SiOC ceramics. Int J Appl Ceram Technol. 2023;20:141–152. https://doi.org/10.1111/ijac.14173